Effects of solute and vacancy segregation on antiphase boundary migration in stoichiometric and Al-rich Fe_3Al: a phase-field simulation study

Yuichiro Koizumi[1]*, Samuel M. Allen[2], Masayuki Ouchi[1] and Yoritoshi Minamino[1]

[1] *Department of Adaptive Machine Systems, Osaka University, 2-1 Yamadaoka, Suita, Osaka, Japan*

[2] *Department of Materials Science and Engineering, Massachusetts Institute of Technology, Cambridge, MA, USA*

ABSTRACT

Effects of segregation of solute atoms and vacancies on migration of antiphase domain boundaries (APDBs) in stoichiometric (Fe-25at%Al) and Al-rich (Fe-28at%Al) Fe_3Al at 673 K have been studied using a phase-field method in which local vacancy concentration is taken into account [Koizumi Y, Allen SM, MinaminoY. Acta Mater 2008;56:5861, *ibid*. 2009;57;3039]. Boundary mobility (*M*) of APBs having different phase-shift vectors of a/4<111> and a/2<100> (hereafter denoted as *B*2-APB and *D*0_3-APD, respectively) were evaluated by measuring the boundary velocity of shrinking circular APDs. Similar effects of the segregations on the migration of *B*2-APBs were observed in both compositions. Vacancies segregated and Al-atoms were depleted at *B*2-APBs in both compositions. Vacancy concentration at *B*2-APBs was up to 80 % higher than those in the bulk. As a result, the migration of *B*2-APBs was greatly enhanced by the vacancy segregation. In contrast, the segregations to *D*0_3 APBs greatly depended on the composition. Vacancies are depleted and Al-atoms segregated at *D*0_3-APBs in the Al-rich Fe_3Al, whereas vacancies segregated and Al-atoms were depleted at *D*0_3-APB in the stoichiometric Fe_3Al. The Al segregation in the Al-rich Fe_3Al decreased the *M* of *D*0_3-APB s much more significantly than the Al-depletion in the stoichiometric Fe_3Al. As the APDs shrank, *D*0_3-APBs broke away from the segregation atmospheres and the *M*s increased rapidly in both compositions. A greater increase in the *M* due to the breakaway was observed in the Al-rich Fe_3Al than in the stoichiometric one.

Keywords: A. iron aluminides (based on Fe_3Al); B. order/disorder transformations; D. antiphase domains; E. simulations

*Corresponding author. Tel: 81-6-6879-7434, Fax: 81-6-6879-4174, e-mail: koizumi@ams.eng.osaka-u.ac.jp

1. Introduction

Antiphase boundaries (APBs) play important roles in plastic deformations of intermetallic compounds. It has been well known that APBs between dissociated superpartial dislocations are responsible for the characteristic mechanical properties such as planar slip at ambient temperature, anomalous temperature dependence of yield stress, abnormal strain-rate dependence of flow stress and so on [1]. Furthermore, recently, it is being revealed that thermal APBs, i.e. antiphase domain boundaries (APDBs) introduced during the course of ordering transformation, significantly affect the mechanical properties of some intermetallic compounds. For instance, the yield stress of Ti_3Al deforming by its primary slip system ($\{1\bar{1}00\}<11\bar{2}0>$ prism slip) can be increased up to 6 times larger than that of a fully ordered single domain crystal by introducing very fine antiphase domains (APDs) of approximately 30 nm average size [2, 3]. APDBs in Fe_3Al have been known to affect the tensile properties [4]. More recently, APDBs in Fe_3Al are attracting increasing interests for their roles in the pseudo-elasticity which is not based on martensitic transformation [5-9]. Because those properties are sensitive to the density of APDBs, or size of APDs, it is important to control APD size appropriately for optimization of mechanical properties. For using APD containing materials at elevated temperatures, the thermal stability of APDs is very important. For controlling the density and distribution of APBs and predicting their thermal stabilities, it is important to understand the kinetics of APB migration.

Phase-field simulation has become a powerful method for simulating micro-structural evolution because of its ability to reproduce complicated morphologies easily [10]. However, at this moment, its applicability for predicting micro-structural evolution in real-time scale is questionable because of the following reason. Generally, phase-field simulation is conducted by solving the Cahn-Hilliard equation [11] for evolving concentration field and the Allen-Cahn equation [12] for evolving the field of non-conservative parameter such as degree of order and crystalinity. Each equation involves kinetic parameter which determines the rate of microstructural evolution. For many binary alloy systems, diffusivity data are available, and the kinetic parameter for the Cahn-Hilliard equation can be derived from the diffusivity data. However, kinetic parameters for phase transformation are available only for limited cases. Sometimes such parameters were determined by fitting simulation results to experimental results. However, such an approach is problematic when the kinetics of micro-structural evolution is dominated by factors which we do not recognize. For instance, we detected segregation of solute atoms on APBs in Ti_3Al [13]. Such segregation may

cause solute-drag and affect apparent mobility of APDBs. Furthermore, it was observed that voids were formed along thermal APBs in CuZn [14]. This implies that vacancies segregate at APBs, and such vacancy segregation may accelerate boundary migration by enhancing the atomic rearrangement near the boundaries. If the effects of segregation are significant, it is quite difficult to determine the kinetic parameters by fitting simulation results to experimental results. Migration of APBs in Fe_3Al may also be affected by such segregations., the relation between APD size and annealing time in Fe-28at%Al alloy annealed at 673 K deviated from the parabolic-law which is theoretically derived for the ideal curvature driven growth of APDs [15]. This deviation may be due to some segregation. For shedding light on the effects of vacancy segregation, we developed a phase-field model in which local vacancy concentration was taken into account [16, 17]. In the latest study [17], we performed simulations of APB migration in the stoichiometric Fe_3Al, and found that the migration of $B2$-APB and $D0_3$-APB were affected by solute and vacancy segregation in different manners [17]. We have demonstrated that the segregation trend changes significantly depending on the alloy composition [16]. Therefore, it is strongly anticipated that the effect of segregation on APB migration depends on the alloy composition. In the present study, we performed simulations of migration of APBs in stoichiometric Fe_3Al (Fe-25at%Al) and Al-rich Fe_3Al (Fe-28at%Al) focusing on the effects of solute segregation and vacancy segregation and their dependence on alloy composition.

2. Method

Since the details of the phase-field model we developed are available in the previous papers [16, 17], only the characteristics of our model are briefly described here. The model we developed is based on the Bragg-Williams model. First, we defined four sublattices and described $B2$-type (η_{B2}) and $D0_3$-type (η_{D03}) long-range order (LRO) parameters by using the probabilities of finding Al atoms in each sublattice. For calculating the probability of finding aluminum, the site fraction of aluminum atoms instead of Al concentration was used taking into account the vacancies. The probability of finding vacancy was defined as a function of $B2$-LRO for reproducing the experimental fact that vacancies preferentially occupy Fe-sites in the nearest neighbor of Al-atom in $B2$-type ordered structure [18]. Internal energy was calculated by using two-body interaction energy given in the literature [19]. The configuration entropy for vacancies was added to the entropy term, and the product of vacancy formation enthalpy and vacancy concentration was added to the enthalpy term. For calculating the energy of non-uniform systems containing interfaces, gradient-energy terms which

determine the interfacial energy, are required. We derived gradient-energy coefficients which were required for calculating gradient-energy, theoretically in the context of the Bragg-Williams model. The gradient-energies for Al-concentration and vacancy concentration were neglected because their contributions to the total free energy were negligibly small compared to those for LRO parameters.

The Al concentration field and LRO fields were evolved by solving one Cahn-Hilliard equation for Al-concentration and two Allen-Cahn equations for *B*2-LRO and $D0_3$-LRO simultaneously. We used kinetic parameters derived from the experimental data of order-order relaxation temporarily [20]. The vacancy concentration field was evolved so that the diffusion potential for vacancy concentration was uniform throughout the simulation box assuming that the mobility of vacancies were much larger than those of Fe- and Al- atoms. Two cases of simulations were performed for each APD-type and each alloy composition in order to examine the effects of vacancy concentration. In one case, each kinetic parameter was assumed to be constant. In another case, the kinetic parameters were assumed to be proportional to the local vacancy concentration considering that atomic rearrangements become faster with increasing vacancy concentration. Hereafter, these two cases are denoted as c_v-independent and c_v-dependent case respectively. The effects of vacancy segregation were examined by comparing the results of these cases. The conditions for the simulations are as follows. Two bulk compositions of Fe-25at%Al (stoichiometric) and Fe-28at%Al (Al-rich) were selected for examining the effect of off-stoichiometry. We generated circular APDs of 11.2 nm radius having an initial segregation atmosphere identical to that of equilibrated planar APBs [16]. Both *B*2-APBs and $D0_3$-APBs, whose phase-shift vectors were a/4<111> and a/2<100> respectively, were examined. Shrinking behaviors of such APDs at a $D0_3$-ordering temperature of 673 K were observed.

3. Results and Discussion

Fig. 1 shows the snapshots of LRO field (Fig. 1a, d), Al concentration field (Fig. 1b, e) and vacancy concentration field (Fig. 1c, f) around a $D0_3$-APDs (**R**=1/2<100>) shrinking at 673 K in stoichiometric Fe_3Al (Fe-25at%Al) (Fig. 1a-c) and Al-rich Fe_3Al (Fe-28at%Al) (Fig.1 d-f). Initial APD radii (r) were 11.2 nm and the time from the beginning of the simulation is 30 ks in both cases. In the stoichirometric Fe_3Al, the APD radius has decreased to about 7.5 nm (Fig. 1a). Aluminum was slightly depleted near the initial position of the APB (r =11.2 nm). Vacancies segregated at the APB while there was also a weak vacancy segregation at the position where the weak

Al-depletion was (Fig. 1c). In contrast, in the Al-rich Fe_3Al (Fig. 1d-f), the APD radius was still as large as 10.5 nm (Fig. 1c) and there are strong Al segregation (Fig. 1e) and vacancy depletion (Fig. 1f) in the vicinity of the APB.

Fig. 2 shows the profiles of vacancy concentration and Al-concentration across the migrating *B*2-APB at various radii. In stoichiometric Fe_3Al, vacancies segregated and Al-atoms were depleted at both *B*2- and $D0_3$-APB, and the segregation atmosphere followed the APB until the APD disappeared by shrinking to zero radius. In the case of $D0_3$-APD (Fig. 3), APBs broke away from segregations as the APDs shrank in both compositions. After the breakaway, Al segregation and depletion are seen respectively ahead and behind of the APB in the stoichiometric Fe_3Al (clearly seen at r = 5 nm in Fig. 3a). The Al segregation and depletion are exchanged in the Al-rich Fe_3Al (Fig. 3b). These profiles of coupled segregation and depletion are analogous to the steady state profile known for migrating planar boundaries [21] although shrinking circular boundaries never reach steady state because the driving force and drag force change with decreasing APD size (i.e. increasing curvature), APB area and accordingly the segregation profiles change at all times. Actually, the segregation and depletion abated with decreasing APD radius (compare the profiles for r = 3 nm and r = 5nm).

Fig. 4 shows the changes in radii of APD with time. The radius of *B*2-APD (Fig. 4a) changed faster in the c_v-dependent case than in the c_v-independent case in both compositions. This can be regarded as a result of enhancement of atom rearrangement near the boundary by the segregated vacancies (Figs. 2b and d). The difference between the rates of radius changes for $D0_3$-APD (Fig. 4b) in the c_v-dependent and c_v-independent cases were much less significant compared to those for *B*2-APD in both compositions. However, it should be noted that the radius change for $D0_3$-APB in the Al-rich Fe_3Al was faster in the c_v-independent case than in the c_v-dependent case in contrast with all the other cases of APB-types and alloy compositions investigated. This is due to the vacancy depletion at $D0_3$-APD in the Al-rich Fe_3Al (Fig. 3d). In the Al-rich Fe_3Al, the APD shrank very slowly compared to that in the stoichiometric Fe_3Al. Also, the radius changes for $D0_3$-APD in the Al-rich Fe_3Al were characteristic in the sense that they appeared to consist of two different parabolic curves connected by knees as indicated by an arrow while the radius changes for other cases appeared to consist of a single parabolic curve. Whereas it appears that the radius decreased following the parabolic-law from the beginning in the stoichiometric Fe_3Al, there was a transition from a very slowly shrinking stage to a rapidly shrinking stage in the Al-rich Fe_3Al. From the changes of APD radius (r), the boundary mobilitiy (M) were evaluated by using the following equation

$$M = (\mathrm{d}r/\mathrm{d}t) / (1/r). \quad (2)$$

Fig. 5 shows the M plotted against APD radius. When a boundary migration is not affected by any external force such as drag force by solute segregation atmosphere, the M is anticipated to be equal to the intrinsic boundary mobilities $M_h^{\mathrm{intrinsic}}$ which is theoretically derived by the Allen-Cahn theory [12]

$$M_h^{\mathrm{intrinsic}} = 2\kappa_h\alpha_h \quad (3)$$

where κ_h is the gradient-energy coefficient and α_h is the kinetic parameter for the Allen-Cahn equation for order parameter h (η_{B2} or η_{D03}). The values of $M_h^{\mathrm{intrinsic}}$s are indicated by dashed horizontal lines. Although the migration of $B2$-APD was enhanced by the vacancy segregation, the $M_{\eta_{B2}}$ for $B2$-APD were much lower than the $M_{\eta_{B2}}^{\mathrm{intrinsic}}$ (Fig. 5a). The difference between the $M_{\eta_{B2}}^{\mathrm{intrinsic}}$ and the simulated $M_{\eta_{B2}}$ is ascribed to the solute-drag arising from the Al-atom depletion (Figs. 2a and c). In the case of $D0_3$-APD (Fig. 5b), the effect of c_v-dependence is much less significant compared to the case of the $B2$-APD in both compositions alloys in accordance with the less significant vacancy segregation (Figs. 3b and d).

In the stoichiometric Fe_3Al, the $M_{\eta_{D03}}$ evaluated from the radius change was lower than the $M_{\eta_{D03}}^{\mathrm{intrinsic}}$ by approximately 40 % at the beginning of the simulation. It increased to reach the $M_{\eta_{D03}}^{\mathrm{intrinsic}}$ when the r was approximately 7 nm. The value of about 7 nm can vary depending on the initial APD radius according to the result of our ongoing calculation. In Al-rich Fe_3Al, the M for the initial stage was only one tenth of the $M_{\eta_{D03}}^{\mathrm{intrinsic}}$. After showing constant value for a while, it increased rapidly to approach the $M_{\eta_{D03}}^{\mathrm{intrinsic}}$. These rapid increases of Ms are ascribed to the breakaway of APBs from the segregation atmosphere (Fig. 3a and c). After the rapid increase, the $M_{\eta_{D03}}$ became almost constant until the r became as small as 1 nm. The effect of decrease in the magnitudes of the segregation and depletion after the breakaway on the $M_{\eta_{D03}}$ (Fig. 3a and c) appears to be negligibly small although some increase is expected in analogy to the theory of impurity drag [21].

Thus, the M for APB migration can be affected by both solute- and vacancy-segregation, and the effects of segregation varies greatly depending on both alloy composition and APB type. For determining accurate kinetic parameters for long-range ordering by fitting a simulated boundary mobility to an experimentally observed one, it is necessary to take into account there effects of segregation. The comparisons of these simulation results with experimentally observed APB migrations for examining the reliability of the kinetic parameters derived by taking into account the segregation is under progress.

Summary

Effects of solute and vacancy segregation on migration of APBs in the stoichiometeric Fe_3Al (Fe-25at%Al) and an Al-rich Fe_3Al (Fe-28at%Al) at 673 K have been studied by a phase-field simulation developed in the previous study. Important results are:

• Fe-atoms and vacancies both segregated to *B*2-APB in both compositions. Vacancy concentrations at the *B*2-APB was more than 60 % higher than those in the bulk. The migration of *B*2-APB was greatly enhanced by the vacancy segregation.

• Al-atoms segregated and vacancies were depleted at $D0_3$-APB in the Al rich Fe_3Al whereas Al-atoms were depleted and vacancies segregated at $D0_3$-APB in the stoichirometric Fe_3Al. The Al segregation in the Al-rich Fe_3Al decreased the boundary mobility of the $D0_3$-APB by solute drag much more significantly than the Al-depletion in the stoichiometric Fe_3Al alloy.

• It is problematic to determine kinetic parameter for ordering transformation by fitting simulation results to experimental results without taking into account the effect of segregation demonstrated in the present study.

Acknowledgements

The present work was supported by the Iketani Science and Technology Foundation.

References

[1] Yamaguchi M, Umakoshi Y. Progress in Materials Science 1990;34:1.
[2] Koizumi Y, Minamino Y, Nakano T, Umakoshi Y. Philos Mag 2008;88:465
[3] Koizumi Y, Minamino Y, Tsuji N, Nakano T, Umakoshi Y. MRS Symp Proc 2003;753:267.
[4] Yoshimi K , Terashima H , Hanada S . Mat Sci Eng A 1995;194:53.
[5] Yasuda HY, Nakajima T, Murakami S, Ueda M, Umakoshi Y. Intermetallics 2006;14:1221.
[6] Yasuda HY, Nakajima T, Nakano K, Yamaoka K, Ueda M, Umakoshi Y. Acta Mater 2005;53:5343.
[7] Yasuda HY, Nakajima T, Umakoshi Y. Scripta Mater 2006;55:859.
[8] Yasuda HY, Nakajima T, Umakoshi Y. Intermetallics 2007;15:819.
[9] Yasuda HY, Nakano K, Nakajima T, Ueda M, Umakoshi Y. Acta Mater 2003;51:5101.
[10] Chen LQ. Ann. Rev Mater Res 2002; 32:113.
[11] Cahn JW , Hilliard JE . J Chem Phys 1958 ;28 :258 .

[12] Allen SM, Cahn JW. Acta Metal 1979;27:1085.
[13] Koizumi Y, Katsumura H, Minamino Y, Tsuji N, Lee JG, Mori H. Sci Tech Adv Mater 2004;5:19.
[14] Cupschalk SG, Brown N. Acta Metall 1968;16:657.
[15] Koizumi Y, Hagiwara T, Minamino Y, Tsuji N. MRS Symp Proc 2005;842:S5.20 .
[16] Koizumi Y, Allen SM, Minamino Y. Acta Mater 2008;56:5861.
[17] Koizumi Y, Allen SM, Minamino Y. Acta Mater 2009;57:3039.
[18] Jiraskova Y, Schneeweiss O, Sob M, Novotny I, Prochazka I, becvar F, Sedlak B. J de Phys IV Colloque C1, supplement au J de Phsique III 1995;5.
[19] Park W. Migration Kinetics of Antiphase Boundaries in Fe-Al Ordered Alloys. Ph D thesis, Department of Materials Science and Engineering, Massachusetts Institute of Technology, Boston 1988.
[20] Oki K, Masuda J, Hasaka M. Trans Japan Inst Metals 1975;6:589.
[21] Cahn JW. Acta Metall 1962;10:789.

Figure Captions

Fig. 1 Snapshots of LRO field (a, d), Al concentration field (b, e) and vacancy concentration field (c, f) around $D0_3$-APDs (**R**=1/2<100>) shrinking at 673 K in the stoichiometric Fe_3Al (Fe-25at%Al) (a-c) and in the Al-rich Fe_3Al (Fe-28at%Al) (d-f). Initial APD radii were 11.2 nm and the time from the beginning of the simulation is 30 ks in both cases.

Fig. 2 Profiles of vacancy concentration (c, f) around *B*2-APDs (**R**=1/4<111>) shrinking at 673 K in stoichiometric Fe_3Al (Fe-25at%Al) and Al-rich Fe_3Al (Fe-28at%Al). Initial APD radii were 11.2 nm and the time from the beginning of the simulation is 30 ks in both cases.

Fig. 3 Profiles of vacancy concentration (c, f) around $D0_3$-APDs (**R**=1/2<100>) shrinking at 673 K in stoichiometric Fe_3Al (Fe-25at%Al) and Al-rich Fe_3Al (Fe-28at%Al). Initial APD radii were 11.2 nm and the time from the beginning of the simulation is 30 ks in both cases.

Fig. 4 Radii of shrinking circular APDs in stoichiometric Fe_3Al (Fe-25at%Al) and Al-rich Fe_3Al (Fe-28at%Al) as a function of annealing time at 673 K. (a) *B*2-APD, (b) $D0_3$-APD.

Fig. 5 Boundary mobilities of shrinking circular APDBs in stoichiometric Fe_3Al (Fe-25at%Al) and Al-rich Fe_3Al (Fe-28at%Al) as a function of APD radius. (a) *B*2-APD, (b) $D0_3$-APD.

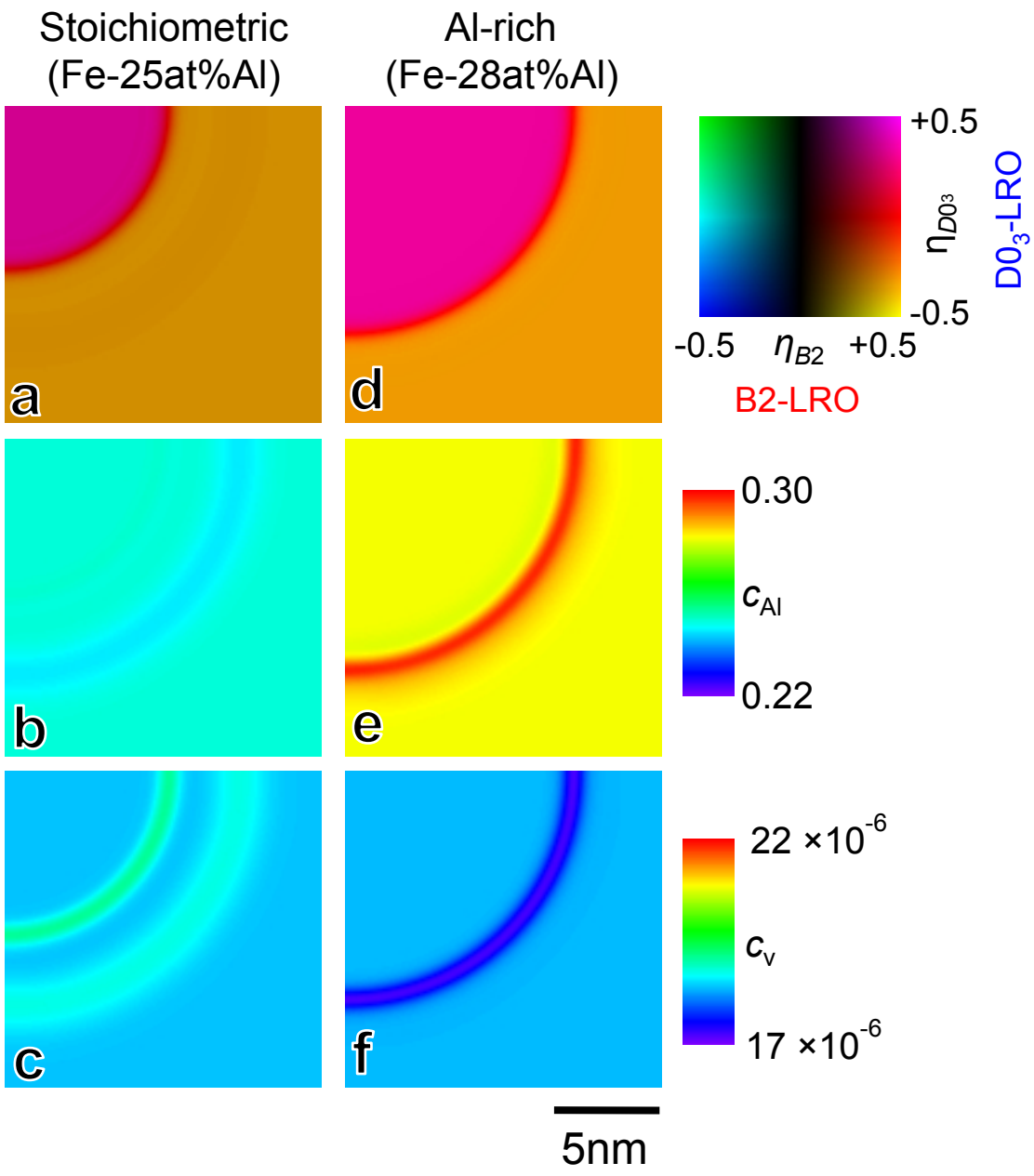
Stoichiometric
(Fe-25at%Al)
Al-rich
(Fe-28at%Al)
a
d
b
e
c
f
+0.5
η_{D0_3}
-0.5
$D0_3$-LRO
-0.5
η_{B2}
+0.5
B2-LRO
0.30
c_{Al}
0.22
22 ×10^{-6}
c_v
17 ×10^{-6}
5nm

Fig. 1

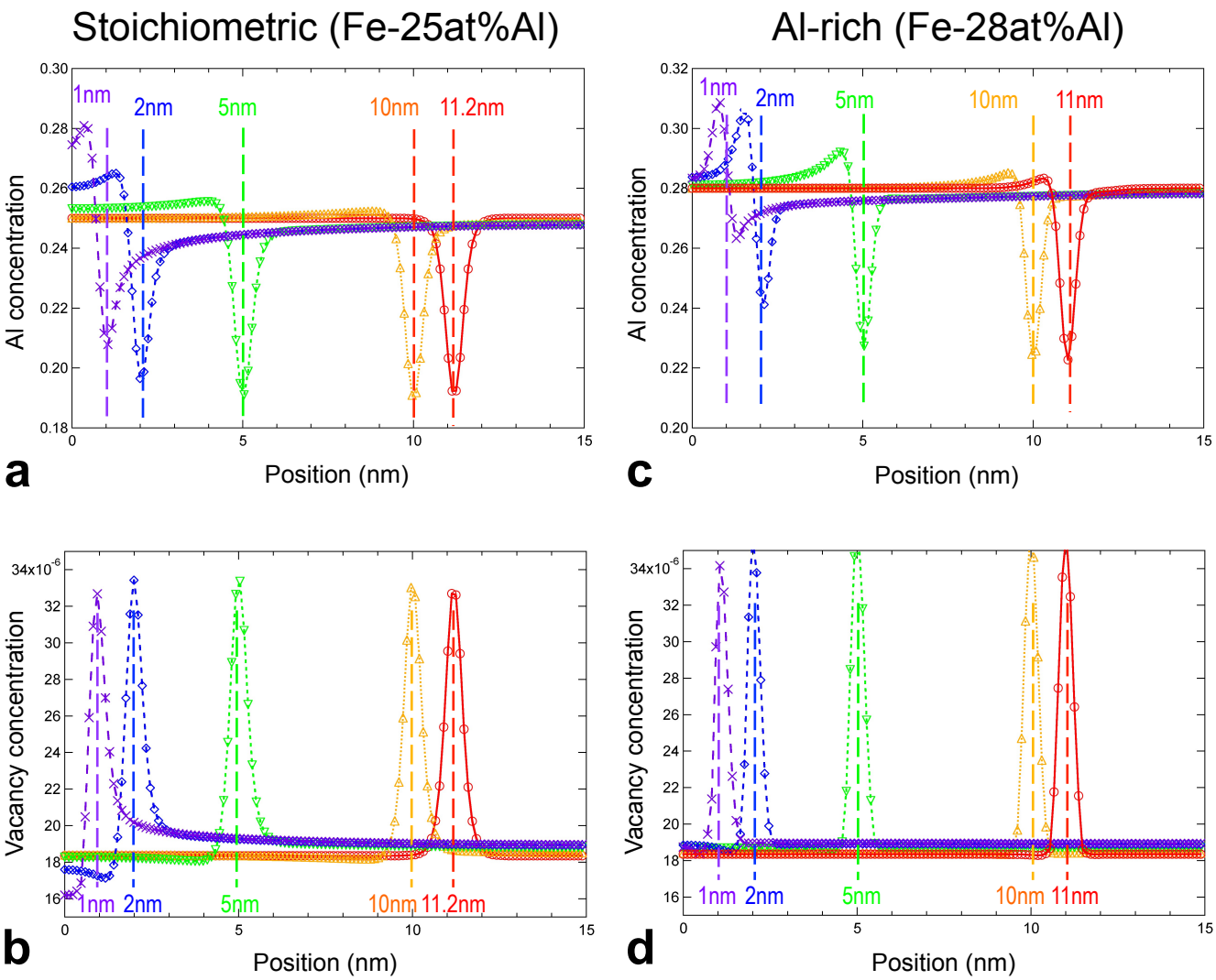
Stoichiometric (Fe-25at%Al)
Al-rich (Fe-28at%Al)
1nm
2nm
5nm
10nm
11.2nm
11nm
Al concentration
Vacancy concentration
34x10-6
Position (nm)
a
b
c
d

Fig. 2

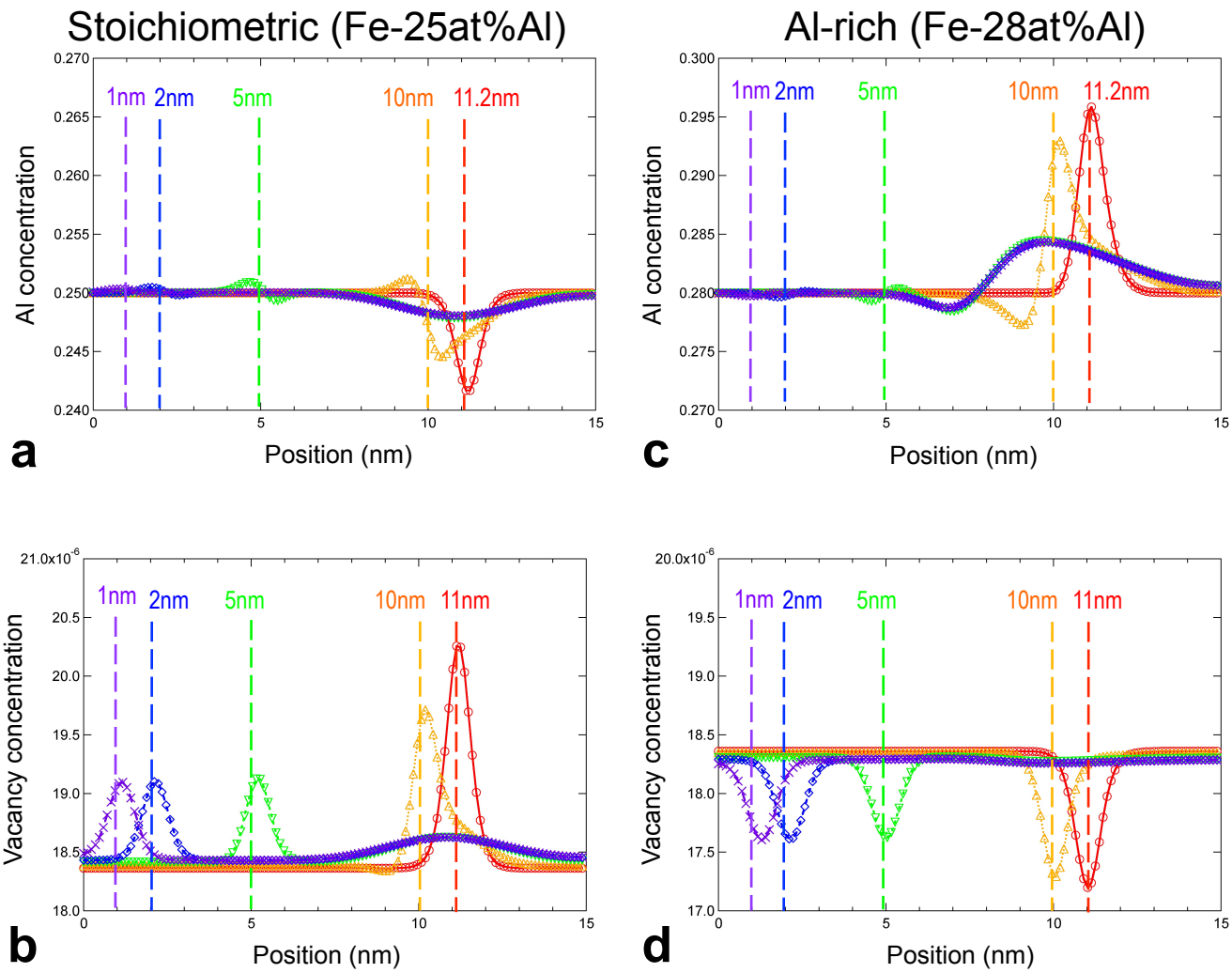
Stoichiometric (Fe-25at%Al)
Al-rich (Fe-28at%Al)
Al concentration
Vacancy concentration
Position (nm)
1nm
2nm
5nm
10nm
11.2nm
11nm
a
b
c
d

Fig. 3

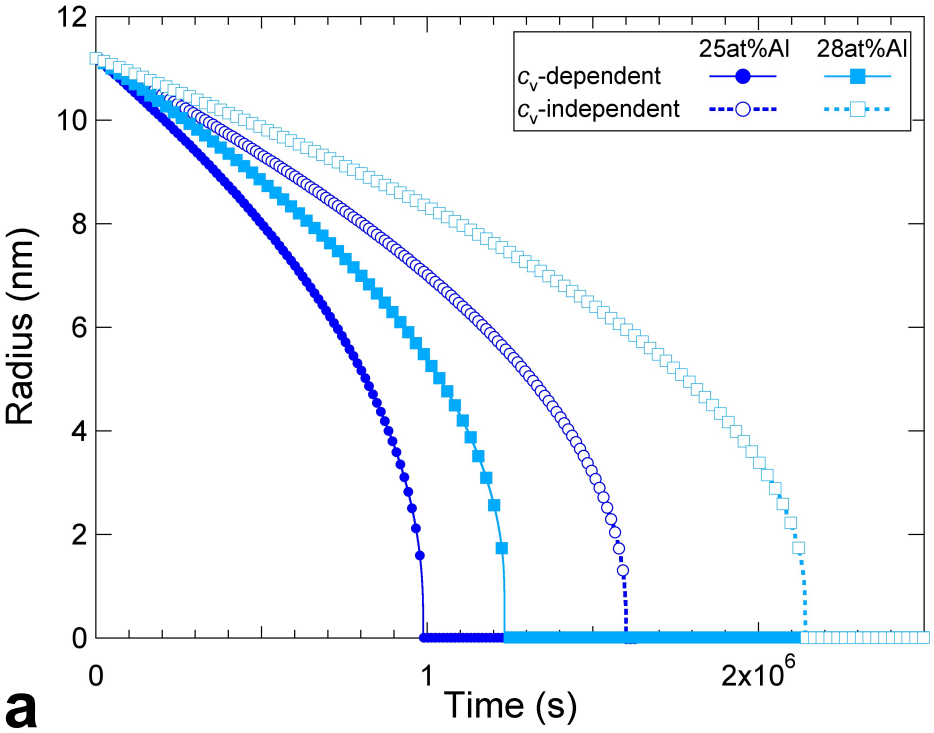
12
10
8
6
4
2
0
Radius (nm)
0
1
2x10^6
Time (s)
25at%Al
28at%Al
c_v-dependent
c_v-independent

a

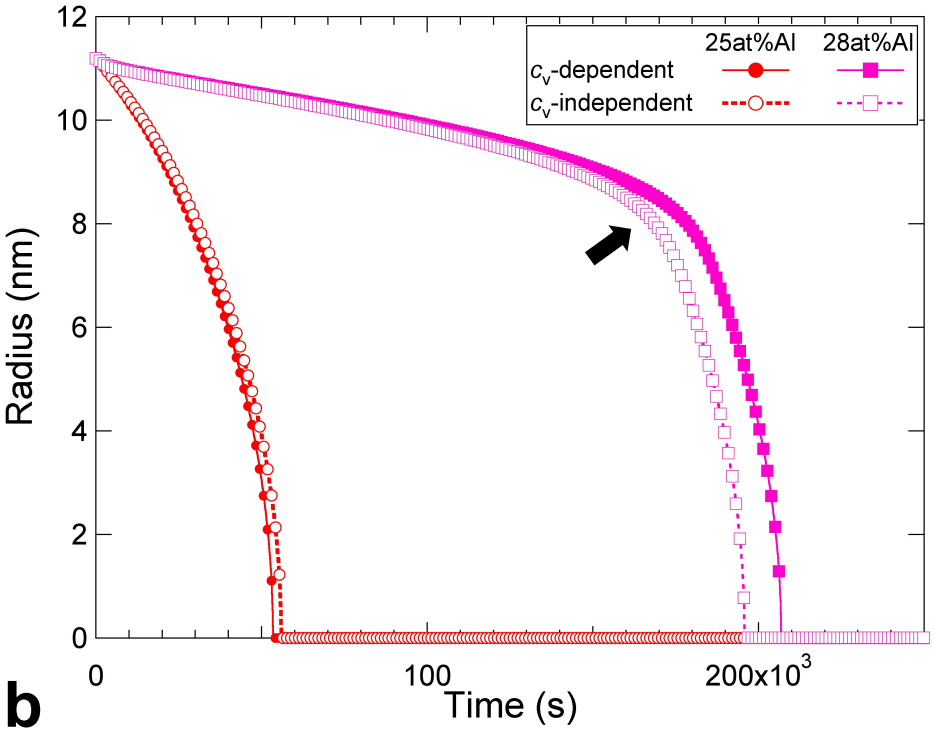
12
10
8
6
4
2
0
Radius (nm)
0
100
200x10^3
Time (s)
25at%Al
28at%Al
c_v-dependent
c_v-independent

b

Fig. 4

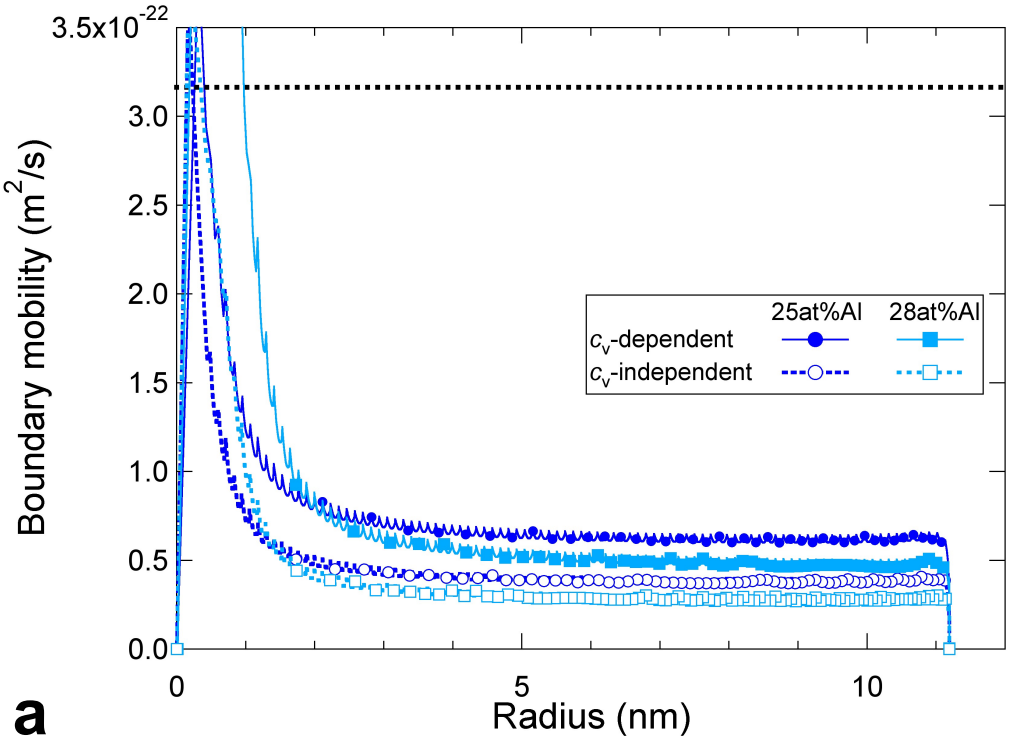
3.5x10-22
3.0
2.5
2.0
1.5
1.0
0.5
0.0
Boundary mobility (m2/s)
0
5
10
Radius (nm)
25at%Al
28at%Al
cv-dependent
cv-independent

a

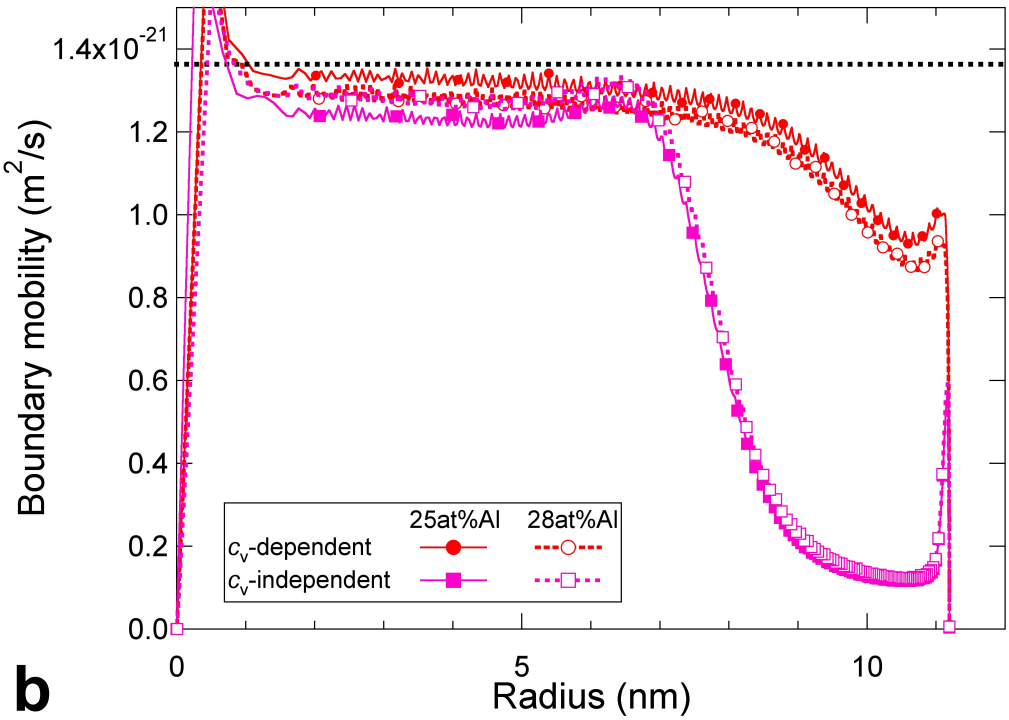
1.4x10-21
1.2
1.0
0.8
0.6
0.4
0.2
0.0
Boundary mobility (m2/s)
0
5
10
Radius (nm)
25at%Al
28at%Al
cv-dependent
cv-independent

b

Fig. 5

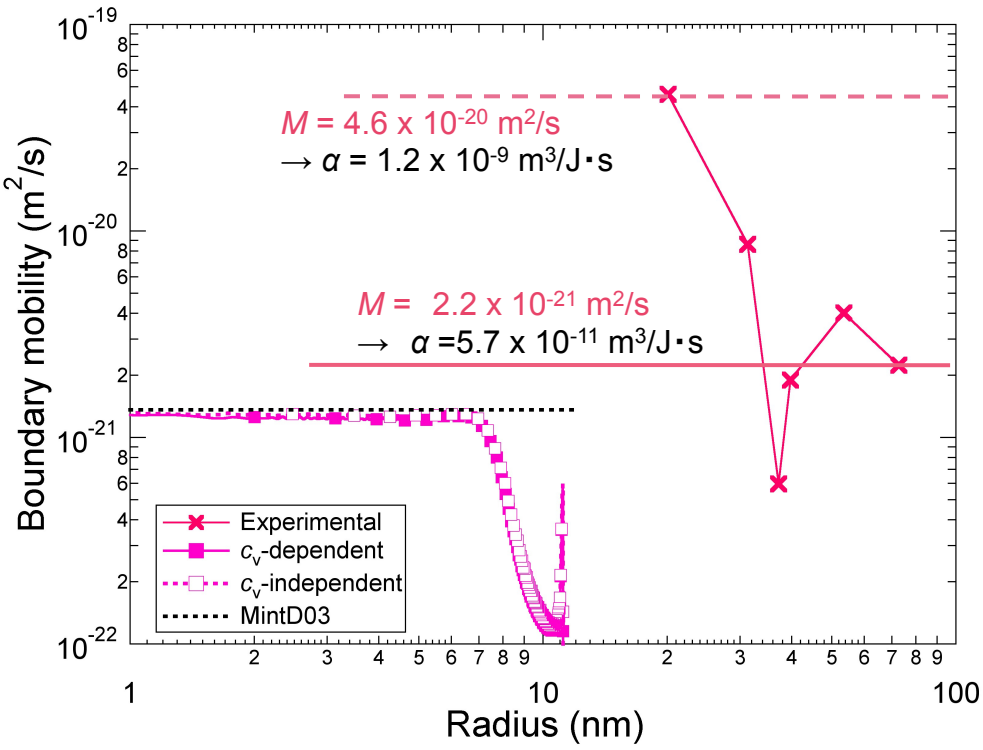
Boundary mobility (m²/s)
Radius (nm)
M = 4.6 x 10⁻²⁰ m²/s
→ α = 1.2 x 10⁻⁹ m³/J·s
M = 2.2 x 10⁻²¹ m²/s
→ α =5.7 x 10⁻¹¹ m³/J·s
Experimental
c_v-dependent
c_v-independent
MintD03

Fig. 6